Journal of Sound and Vibration 326 (2009) 522–539

Contents lists available at ScienceDirect

Journal of Sound and Vibration

journal homepage: www.elsevier.com/locate/jsvi

Estimation of modal loads using structural response

Jae-seung Hwang [a,*], Ahsan Kareem [b], Wha-jung Kim [c]

[a] School of Architecture, Chonnam National University, Gwangju 500-757, Republic of Korea
[b] NatHaz Modeling Laboratory, Department of Civil Engineering and Geological Sciences, University of Notre Dame, Notre Dame, IN 46556, USA
[c] School of Architecture & Civil Engineering, Kyungpook National University, Daegu 702-701, Republic of Korea

ARTICLE INFO

Article history:
Received 29 December 2007
Received in revised form
30 April 2009
Accepted 3 May 2009
Handling Editor: L.G. Tham
Available online 6 June 2009

ABSTRACT

In this study an analytical procedure is developed based on the Kalman filtering approach to estimate modal loads applied on a structure using limited measured response of the structure. The effect of various variables such as the type of response, the noise level, and the level of uncertainty in dynamic properties of the structure, on the modal load estimation is evaluated in the frequency domain through numerical analysis for a single-degree-of-freedom (SDOF) and a multi-degree-of-freedom (MDOF) system. It is observed that the acceleration response is relatively more stable and robust in external load estimation than other response components. The noise is amplified at the high frequency range for the displacement or velocity response whereas in the case of acceleration response the noise is not amplified in the estimated external load. It is also found that the discrepancy between dynamic characteristics derived for an analytical model and the actual structure causes the transfer function from the actual load to the estimated load to distort near and below the structural natural frequency. The estimation of external loads is extended to a MDOF system. The results show that the modal loads can be estimated accurately from limited measurements of acceleration response on the basis of the assumption that the measured response can be transformed to the modal response by a proper orthogonal decomposition and the corresponding modal properties used for the transformation can be obtained by a system identification technique.

1. Introduction

Mathematical models for dynamic loads acting on a building structure have been developed in design code around the world for the analysis and design of structures [1–4]. Such mathematical models often may not be accurate due to the uncertainties inherent in the associated loads and the underlying mathematical models. Furthermore, there are cases in which no mathematical models are available because the external loads such as wind loads are too complex to be expressed in a closed analytical form. In such cases experiments are generally carried out to simulate the loads [5,6].

More reliable mathematical models for dynamic loads can be obtained if they are constructed using a high frequency force balance or synchronously measured pressure on a model surface. Such direct measurements of the excitation may have an advantage in that the mathematical model is formulated based on reliable data; however it needs extensive measurements program requiring elaborate wind tunnel and transducing systems. In full-scale measurements, it is not feasible to measure directly loads applied on a structure. Therefore, it would be useful if the external loads can be estimated

* Corresponding author. Tel.: +82 62 530 1641; fax: +82 62 530 0250.
E-mail address: jshwang@jnu.ac.kr (J.-s. Hwang).

0022-460X/$ - see front matter © 2009 Elsevier Ltd. All rights reserved.
doi:10.1016/j.jsv.2009.05.003

Nomenclature

A	$2n \times 2n$ dimensional system matrix
B	$2n \times n$ dimensional system matrix
B^+	generalized inverse of matrix B
C	$p \times 2n$ dimensional system matrix
C_o	$n \times n$ damping matrix
C_{oi}	i-th modal damping
D	$p \times n$ dimensional system matrix
e	error between state variable and estimate variable
E	expectation sign
f	n-dimensional external load
$\hat{f}$	estimated load
F_i	i-th modal load
I	unit matrix
K	Kalman filter gain
K_i	i-th modal stiffness
K_o	$n \times n$ stiffness matrix
M	$n \times n$ mass matrix
M_i	i-th modal mass
n	degree of freedom of structure
P	covariance matrix of error
Q_1	covariance matrix of external load
Q_2	covariance matrix of the noise
s	Laplace variable
x	n-dimensional displacement vector
$\ddot{x}_r$	p-dimensional vector of the measured acceleration
y	p-dimensional vector of the measured outputs
$\hat{y}$	p-dimensional vector of the filter output
z	$2n$-dimensional state variable
$\hat{z}$	$2n$-dimensional vector of the estimated variable
γ	the magnitude of covariance matrix of the noise
Δ_1	the error between the exact modal acceleration response and estimated
ε	p-dimensional vector of the noise
η_i	i-th generalized displacement
$\ddot{\eta}_r$	q-dimensional modal acceleration
$\underset{\sim}{\lambda}$	state variable in modal space
$\hat{\lambda}$	estimate variable in modal space
v	output in the modal space
ξ_i	i-th mode's damping ratio
ϕ_i	i-th mode's eigen vector
Φ	$n \times n$ eigen matrix
Φ_r	$p \times q$ eigen matrix
ω_i	i-th mode's natural frequency

indirectly using the response of structure as the direct measurements of the excitation are not available. As a result, indirect estimation of external loads has been attempted, which is an important type of inverse problem involving identification of force from measured structural response.

External load estimation using the structural response has been evolving over several decades in engineering. [7,8] Law et al. [9] developed a method to estimate wind loads and verified the method for estimating wind load acting on a 50 m guyed mast. Lu and Law [10] proposed a method for identifying input excitation using the sensitivity measures of the dynamic response with respect to the input force. Liu and Shepard [11] developed dynamic force identification in the frequency domain based on enhanced least squares approach. The force identification has also been applied for the estimation of moving loads [12–14]. Liu et al. [15] used the inverse algorithm to estimate steady-state sinusoidal and rectangular signals applied on a cantilever plate. Ma et al. [16] and Ma and Ho [17] investigated the problem of force identification of cantilever beam through numerical analysis and applied an inverse method to nonlinear structural systems. Particularly, above three papers [15–17] made valuable contributions to the force identification and their success has provided further impetus for the estimation of external loads. For example, Ref. [15] proposed an estimation method utilizing measured response at a point different from the exciting point based on two distinct state space models (the transfer measurement and the point measurement) realized by a linear identification technique with Markov parameters and ERA realization and verified the feasibility and accuracy of proposed method with laboratory tests. In Ref. [16], the estimation method based on the Kalman filter and a recursive least-squares algorithm was formulated and applied to a multi-degree-of-freedom (MDOF) system constructed by the finite element discretization. The practicability of the estimation method was verified for a cantilever beam subjected to different types of input force, e.g., sinusoidal, triangular, rectangular impulses and random force. Ref. [17] proposes an advanced inverse method which is applicable to nonlinear structural systems. By using the estimation method composed of the extended Kalman filter and recursive least-squares estimator, it was shown that the input forces applied on nonlinear systems with the linear and cubic terms in the spring and damper could be identified successfully.

However, these developments could not be extended in a straight forward manner to systems such as buildings. It was generally assumed in these studies that the mass, stiffness, and damping matrices were known a priori for force identification. But, the finite element model may yield large discrepancy in these features compared to the actual structures and there are limitations when using system identification techniques. Further, the target forces in previous works have been generally point loads acting at a specific DOF while wind loads acting on a building structure space and time. As a result, it is very difficult to construct the state space model using the system identification techniques as used in Ref. [15]. Therefore, it is more useful to perform the load identification in modal space rather than in the physical domain. This implies that it is easier to obtain the natural frequencies, damping ratios, and mode shapes than the respective mass, stiffness, and damping matrices. Typically, the response of a building subjected to the dynamic wind loads is primarily

governed by the first few fundamental modes even though the building has numerous DOFs. In the case of vortex-induced vibration, often the first vibration mode has a significant influence on the response of civil structures and in some cases like tall poles the second mode may come into play. Consequently, the exact estimation of modal loads will provide useful information for the design of buildings or slender structures such as chimney and tower.

Unfortunately, it is also noted that there exist uncertainties in the estimation of natural frequency and damping ratio due to amplitude dependency and a variety of mechanisms responsible towards damping and inherent uncertainties associated with damping estimates. These issues have not been explicitly addressed in previous studies. More recently, both displacement and acceleration measurements have been made possible utilizing a GPS or accelerometer, which may have their individual implications on the estimation of excitation.

In this study a procedure is developed to estimate external modal loads using measured structural response and the Kalman filtering scheme. One of the focuses of this study is to identify the loading associated with a particular mode of vibration with applications to vortex shedding induced loads. In order to treat practical issues that surface in applications, the influence of variables such as the type of measured response, amplitude of associated noise, and the discrepancies in the dynamic properties between the actual and the analytical models on the transfer function from actual load to the estimated load is evaluated in the frequency domain. The estimation method is formulated in a closed-form in the modal space to construct the loading model for structural design. The method is verified through numerical analysis of a single-degree-of-freedom (SDOF) system subject to sinusoidal load representing simplified vortex shedding. In addition, numerical analysis of a MODF system subjected to wind loads is also examined in order to demonstrate the feasibility of the proposed method to large degrees of freedom systems. The method presented here can be further expanded and applied to construct empirical models of dynamic wind load effects to estimate fatigue based on full-scale measurements.

2. Estimation of external loads

2.1. Estimation of loads based on Kalman filtering scheme

In this section, a procedure for the estimation of external loads using the Kalman filtering scheme is introduced. The Kalman filtering has been reported extensively in the literature with mathematical rigor [18]. This study is confined only to the utilization of the basic principles of the Kalman filtering scheme as it applies to the estimation of external loads. The equation of motion of a structure subjected to a disturbance f is generally expressed as

$$M\ddot{x} + C_o\dot{x} + K_o x = f \tag{1}$$

If the response components and system matrices are known, the external load can be computed as

$$f = M\ddot{x} + C_o\dot{x} + K_o x \tag{2}$$

The system matrices, with some degrees of uncertainty, are determined from the finite element models. Generally, however, only a few response components are measurable in practice. In this case, unmeasured responses required for accurate estimation of the external loads can be estimated by the Kalman filter. Accordingly, in order to estimate all variables from the measured output data, the following Kalman filter is utilized.

$$\dot{\hat{z}} = (A - KC)\hat{z} + Ky \tag{3a}$$

$$\hat{y} = C\hat{z} \tag{3b}$$

The matrices A and C are defined in the following state-space form of Eq. (1) [19]:

$$\dot{z} = Az + Bf \tag{4a}$$

$$y = Cz + Df + \varepsilon \tag{4b}$$

The Kalman filter gain is obtained by minimizing the error between the state variable and the estimated variable. The Kalman filter gain can be written as

$$K = (BQ_1D^{\mathrm{T}} + PC^{\mathrm{T}})(DQ_1D^{\mathrm{T}} + Q_2)^{-1} \tag{5}$$

The covariance matrix of the error, P, can be obtained from following Riccati equation:

$$AP + PA^{\mathrm{T}} - (CP + DQ_1B^{\mathrm{T}})^{\mathrm{T}}(DQ_1D^{\mathrm{T}} + Q_2)^{-1} \cdot (CP + DQ_1B^{\mathrm{T}}) + B^{\mathrm{T}}Q_1B = 0 \tag{6}$$

The covariance matrix Q_1 of external load and the covariance matrix Q_2 of the noise are simply assumed as the following, respectively

$$\begin{aligned} Q_1 &= E[ff^{\mathrm{T}}] = I \\ Q_2 &= E[\varepsilon\varepsilon^{\mathrm{T}}] = \gamma I \end{aligned} \tag{7a}$$

By varying the factor γ which represents the magnitude of the covariance matrix of noise, the optimum filter gain K and the covariance matrix P of the filter gain can be estimated. The covariance matrix Q_1 of the external load is assumed to be an identity matrix because the load cannot be known a priori in the process of load estimation

The estimated variables are obtained from the Kalman filter presented in Eq. (3). As the error between the estimated variables and the response of the structure (state variables) decreases, the estimated variables converge to the state variables. Since the convergence depends on γ, the optimal value for γ needs to be obtained by a parametric study. If it is assumed that optimal value for γ is known and the estimated variables converge to the state variables, and then the state equation presented in Eq. (4a) is written as follows:

$$\dot{\hat{z}} = A\hat{z} + B\hat{f} \tag{8}$$

Using the generalized inverse B^+, Eq. (8) can be expressed as

$$\hat{f} = B^+(\dot{\hat{z}} - A\hat{z}) \tag{9}$$

With Eq. (3a), Eq. (9) can be rewritten as

$$\hat{f} = B^+K(y - C\hat{z}) \tag{10}$$

Using Eq. (4b), Eq. (10) can be expressed as

$$\hat{f} = B^+KC(z - \hat{z}) + B^+KDf + B^+K\varepsilon = B^+KCe + B^+KDf + B^+K\varepsilon \tag{11}$$

Eq. (11) suggests that the error, e, and the noise, ε, as well as the actual load, f, influence the estimated load, $\hat{f}$.

2.2. Estimation of external load in modal space

The estimation procedure presented in previous section is applicable only when the mass, stiffness and damping matrices of structure are fully known. For the application to a building or a slender structure in which response is dominated by the first fundamental mode, the estimation method introduced in the previous section can be applied to the single-degree-of-freedom system in modal space. In order to separate all of the modal responses from the measured response of structure, the sensors as many as the number of DOF are needed to be installed in the structure. For example, as the simplest method, based on the condition that acceleration responses of all DOFs, $\ddot{x}$, are measurable and the eigen matrix Φ is available, then the modal acceleration response vector, $\ddot{\eta}$, can be represented as

$$\ddot{\eta} = \Phi^{-1}\ddot{x} \tag{12}$$

In practice, however, due to the limitation on the number of accelerometers and corresponding identified mode shapes, the measured acceleration responses can be approximately represented using the modal acceleration response as follows:

$$\begin{bmatrix} \ddot{x}_1 \\ \ddot{x}_2 \\ \vdots \\ \ddot{x}_p \end{bmatrix} = \begin{bmatrix} \phi_{11} & \phi_{12} & \cdots & \phi_{1q} \\ \phi_{21} & \phi_{22} & \cdots & \phi_{2q} \\ \vdots & \vdots & \ddots & \vdots \\ \phi_{p1} & \phi_{p2} & \cdots & \phi_{pq} \end{bmatrix} \begin{bmatrix} \ddot{\eta}_1 \\ \ddot{\eta}_2 \\ \vdots \\ \ddot{\eta}_q \end{bmatrix} \tag{13}$$

where $\ddot{x}_j$ ($j = 1,\ldots,p$) is the acceleration response at the j-th DOF, $\ddot{\eta}_k$ ($k = 1,\ldots,q$) the k-th modal acceleration, and ϕ_{jk} the (j, k)-th element of identified eigen matrix. In general, the number of modes is larger than that of accelerometers ($q > p$) because modal properties and mode shapes can be obtained from relatively lesser number of acceleration response measurements using system identification techniques. Simply, Eq. (13) can be expressed as

$$\ddot{x}_r = \Phi_r\ddot{\eta}_r \tag{14}$$

where the subscript r implies that the length of the vector is reduced.

From Eq. (14), the modal acceleration responses can be obtained from the measured acceleration responses using the generalized inverse of the matrix, Φ_r^+, as

$$\ddot{\eta}_r = \Phi_r^+\ddot{x}_r \tag{15a}$$

$$\ddot{\eta}_r = \Phi_r^{-1}\ddot{x}_r \quad (\text{if } p = q) \tag{15b}$$

From Eqs. (12) and (15), the error between the exact modal acceleration response and estimated one can be expressed as

$$\Delta_1 = S^{\mathrm{T}}\ddot{\eta} - S_r^{\mathrm{T}}\ddot{\eta}_r = S^{\mathrm{T}}\Phi^{-1}\ddot{x} - S_r^{\mathrm{T}}\Phi_r^{-1}\ddot{x}_r \tag{16}$$

where S and S_r are location vectors used to choose the specific modal acceleration response with appropriate dimension. For example, S can be expressed as $S = [1\ 0\ \ldots\ 0]^{\mathrm{T}}$ in the case of the first modal acceleration response.

The error in Eq. (16) can be minimized by choosing the number of sensors to exceed the number of modes governing the response of structure. In this study, the required number of sensors is determined in such a way that the number of sensors

is larger than that of governing modes whose energy contribution is over 99 percent based on the proper orthogonal decomposition (POD). [20,21] Using the modal response of structure from Eq. (16), Eq. (1) can be transformed to the modal space

$$M_i\ddot{\eta}_i + C_{oi}\dot{\eta}_i + K_i\eta_i = \phi_i^{\mathrm{T}} f = F_i \tag{17}$$

In the modal space, the state space equation and the modal output (v) obtained from acceleration response can be represented as

$$\begin{bmatrix} \dot{\eta} \\ \ddot{\eta} \end{bmatrix} = \begin{bmatrix} 0 & 1 \\ -M_i^{-1}K_i & -M_i^{-1}C_{oi} \end{bmatrix} \begin{bmatrix} \eta \\ \dot{\eta} \end{bmatrix} + \begin{bmatrix} 0 \\ M_i^{-1} \end{bmatrix} F_i \tag{18a}$$

$$v = \ddot{\eta} = [-M_i^{-1}K_i,\ -M_i^{-1}C_{oi}] \begin{bmatrix} \eta \\ \dot{\eta} \end{bmatrix} + M_i^{-1}F_i \tag{18b}$$

$$\lambda = [\eta\ \ \dot{\eta}]^{\mathrm{T}} \tag{18c}$$

$$f_i = F_i/M_i \tag{18d}$$

Using Eq. (18c) and (18d), Eq. (18a) and (18b) can be simplified as

$$\dot{\lambda} = A_i\lambda + B_i f_i \tag{19a}$$

$$v = C_i\lambda + D_i f_i \tag{19b}$$

System matrix A_i, B_i can be written as

$$A_i = \begin{bmatrix} 0 & 1 \\ -\omega_i^2 & -2\xi_i\omega_i \end{bmatrix} = \begin{bmatrix} 0 & 1 \\ -k & -d \end{bmatrix} \tag{20a}$$

$$B_i = \begin{bmatrix} 0 \\ 1 \end{bmatrix} \tag{20b}$$

Matrices C_i, D_i are different depending on the response utilized. These matrices are presented in Table 1.

Following the scheme presented in the previous section, the modal load can be obtained as

$$f_i = B_i^{+}(\dot{\widehat{\lambda}} - A_i\,\widehat{\lambda}) \tag{21a}$$

$$f_i = B_i^{+}K_i(v - C_i\,\widehat{\lambda}) \tag{21b}$$

$\widehat{\lambda}$ is estimate variable of Kalman filter defined in modal space and can be calculated from following Eq. (22).

$$\dot{\widehat{\lambda}} = (A_i - K_iC_i)\,\widehat{\lambda} + Kv \tag{22}$$

The optimal Kalman filter gain K_i can be described in a closed-form in terms of variables γ, k and d in Eq. (20) for SDOF system by substituting the following matrix P_i into Eq. (6) and solving the Riccati equation:

$$P_i = \begin{pmatrix} p_1 & p_2 \\ p_2 & p_3 \end{pmatrix} \quad K_i = \begin{pmatrix} k_1 \\ k_2 \end{pmatrix} \tag{23}$$

The element of matrices P_i and K_i defined in Eq. (23) are presented in Table 2.

Finally, the modal load F_i can be calculated as the product f_i obtained from Eq. (21) and the modal mass M_i. Where, modal mass can be obtained based on system identification procedures, e.g., [22,23].

Table 1
Matrices C and D.

Response	Matrix C	Matrix D
Displacement	(1 0)	0
Velocity	(0 1)	0
Acceleration	$[-\omega_i^2\ \ -2\xi_i\omega_i]$	1

Table 2
Elements of the matrices P and K.

Response	Matrix P	Matrix K
Displacement	$p_1 = x^a$ $p_2 = p_1^2/2\gamma$ $p_3 = kp_1 + dp_2 + p_1p_2/\gamma$	$k_1 = p_1/k,\ k_2 = p_2/\gamma$
Velocity	$p_1 = p_3/k,\ p_2 = 0$ $p_3 = -d\gamma + \sqrt{1+(d\gamma)^2}$	$k_1 = p_2/k,\ k_2 = p_3/\gamma$
Acceleration	$p_1 = (d^2/k^2 + g(\gamma)/k)p_3 + dh(\gamma)/k^{2b}$ $p_2 = p_3^2/2\gamma$ $p_3 = (-d\gamma + \sqrt{(d\gamma)^2 - 2k\gamma h(\gamma)})/k$	$k_1 = p_3\sqrt{1/\gamma(1+\gamma)}$ $k_2 = -\gamma/(1+\gamma) + \sqrt{\gamma/(1+\gamma)}$

[a] $x^4+3d\gamma x^3+4\gamma^2(d^2+k)x^2+8kd\gamma^3x-4\gamma^3 = 0$.
[b] $g(\gamma) = \sqrt{(1+\gamma)/\gamma}$, $h(\gamma) = \gamma - \sqrt{\gamma(\gamma+1)}$.

3. Transfer functions of estimated load

In this section, the influence of the type of response, amplitude of noise, and the discrepancy of dynamic properties between the actual structures and the analytical model on the transfer function from actual load to the estimated load is evaluated in the frequency domain for a SDOF system in modal space. For simplicity, the subscript representing a mode is omitted.

3.1. Sensitivity to the type of response

To evaluate the effect of the type of response used to estimate the external loads in the frequency domain, using Eq. (11) is examined by transforming it by the Laplace transformation.

$$\hat{f}(s) = B^+KCe(s) + B^+KDf(s) + B^+K\varepsilon(s) \tag{24}$$

The error $e(s)$ can be expressed as

$$e(s) = (sI - A + KC)^{-1}(B - KD)f(s) - (sI - A + KC)^{-1}K\varepsilon(s) \tag{25}$$

Substituting Eq. (25) in Eq. (24), the estimated load can be expressed in the frequency domain as

$$\hat{f}(s) = T_e(s)f(s) + T_\eta(s)\varepsilon(s) \tag{26}$$

The transfer function from the actual load to the estimate load, $T_e(s)$, and the transfer function from the noise to the estimate load, $T_\eta(s)$, can be expressed as

$$T_e(s) = B^+K(CT_k(s)(B - KD) + D) \tag{27a}$$

$$T_\eta(s) = B^+K(I - CT_k(s)K) \tag{27b}$$

$$T_k(s) = (sI - A + KC)^{-1} \tag{27c}$$

If there is no noise and the magnitude of the transfer function $T_e(s)$ is unit value for SDOF system in Eq. (26), then the estimated load is identical to the actual load. However, the transfer function varies with the type of the response and the estimated load is invariably contaminated by noise.

In Figs. 1 and 2, the magnitude and phase angle of the transfer function $T_e(s)$ are calculated in the frequency domain by substituting for the Laplace variable 's' by '$i\omega$' (i: complex number, ω: angular velocity). Accordingly, $|T_e(i\omega)|$ and $phase(T_e(i\omega))$ are compared for different type of measured response when $\gamma = 10^{-8}$. The mass, natural frequency, and damping ratio of the SDOF system used in the numerical simulation are presented in Table 3.

It is observed in Fig. 1 that the shape of transfer functions $T_e(s)$ varies with the type of the response. In the case of displacement feedback in which displacement is used to estimate the load, the transfer function decreases rapidly in the high frequency region. Whereas for the acceleration feedback, the transfer function is less than one in the low frequency range. For the velocity feedback, however, the function has a unit value throughout the frequency range.

It can be noted in Fig. 2 that there is no phase lag when the external load is estimated by the velocity feedback. This implies that the velocity feedback is more robust for estimating the load than other response components. Generally, however, measuring the velocity response of structures is not convenient. Therefore, the use of acceleration feedback is the

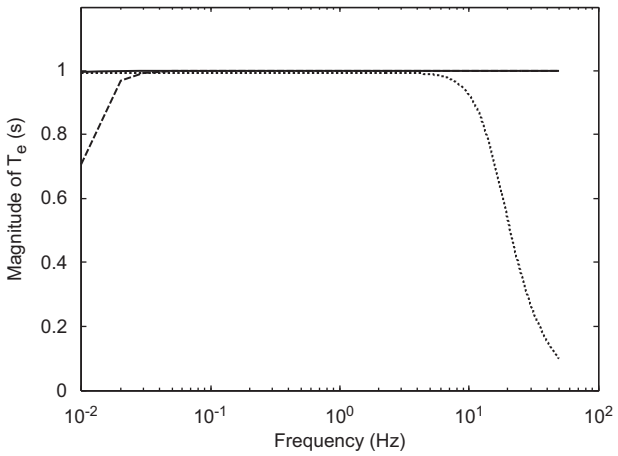

Fig. 1. Magnitude of the transfer functions $T_e(s)$ for different types of responses (solid line: velocity feedback, dashed line: acceleration feedback, dotted line: displacement feedback).

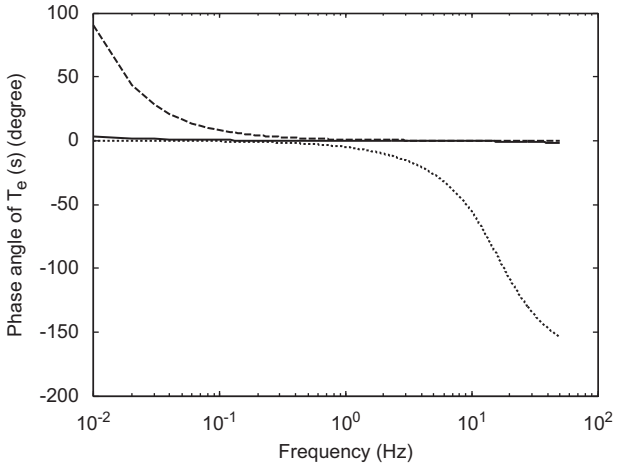

Fig. 2. Phase angle of the transfer functions $T_e(s)$ for different types of responses (solid line: velocity feedback, dashed line: acceleration feedback, dotted line: displacement feedback).

Table 3
Dynamic properties of a SDOF system and Load 1.

Model structure in modal space	Specification
Modal mass	1.0 (mass normalized)
Damping ratio (percent)	1.0
Natural frequency (Hz)	1.0
Analysis condition	Time interval: 0.01 s Duration: 600 s
Noise	
Shape	High pass filtered white noise
Frequency range	over 40 Hz
Transfer function of HPF	$\frac{0.004824s^4 - 152.9s^3 - 11,180s^2 - 8.6\times10^6 s - 2.635\times10^{-5}}{s^4 + 167.5s^3 + 1.572\times10^5 s^2 + 1.192\times10^7 s + 5.645\times10^9}$
Load 1	
Shape	Sine wave
Frequency	The same with the natural frequency of structure

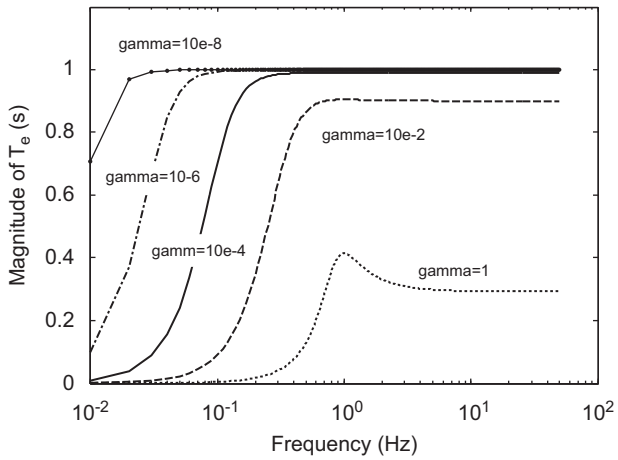

Fig. 3. The effect of the covariance matrix of the noise (γ) on transfer function $T_e(s)$ for acceleration feedback.

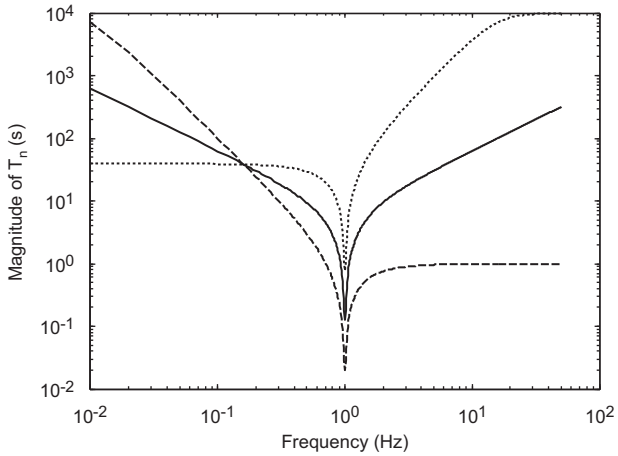

Fig. 4. Magnitude of transfer functions $T_n(s)$ for different types of responses (solid line: velocity feedback, dashed line: acceleration feedback, dotted line: displacement feedback).

most practical option for estimating external loads. As mentioned in Section 2.1, since the accuracy of the transfer function $T_e(s)$ depends on γ, the optimal value for γ needs to be obtained by parametric study. Fig. 3 shows that the transfer function $T_e(s)$ is converging to the exact one as the γ is decreased for the acceleration feedback.

3.2. The effect of noise

Typically full-scale data is corrupted by noise. In order to evaluate the effect of noise on the estimated load, the transfer function from noise to external load given in Eq. (27b) is plotted in Fig. 4 for different types of response when $\gamma = 10^{-8}$. It can be observed that the transfer functions for displacement and velocity feedback are amplified on both sides of the natural frequency, whereas the transfer function for the acceleration response converges units at the frequency range higher than the natural frequency. This implies that the acceleration feedback provides stable estimation of external load because frequency of noise is generally distributed in the high frequency range.

3.3. Sensitivity to dynamic properties

To estimate external loads accurately, reliable estimates of dynamic properties as well as the structural response are needed. Dynamic properties derived from a finite element code may exhibit departure from those measured in the field,

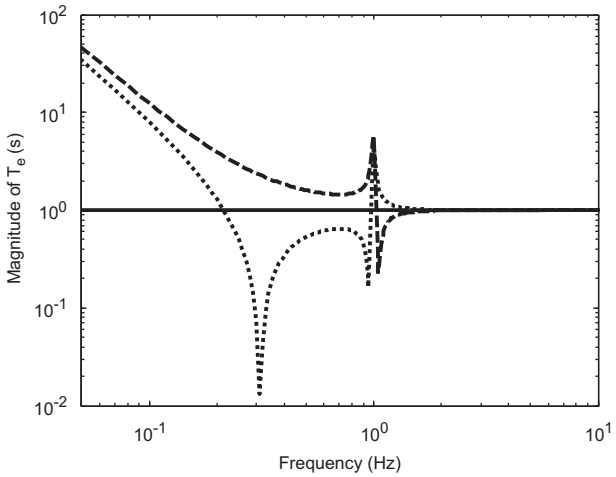

Fig. 5. The effect of discrepancy in natural frequency (solid line: 0% discrepancy, dashed line: +5% discrepancy, dotted line: −5% discrepancy).

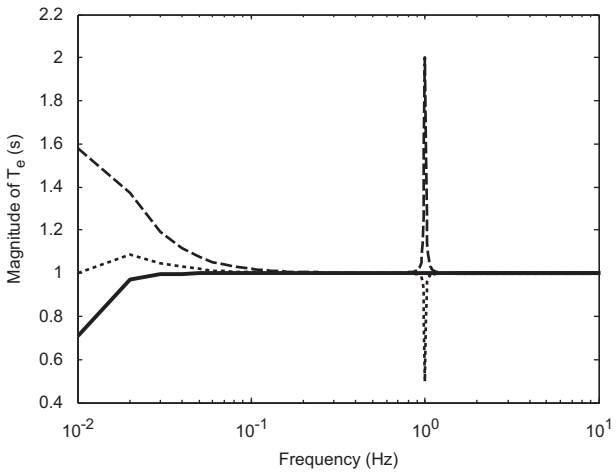

Fig. 6. The effect of discrepancy in damping ratio (solid line: 1% damping (exact), dotted line: 0.5% damping, dashed line: 2% damping).

especially for concrete structures. [24] This discrepancy is reflected in the Kalman filter, therefore, Eq. (3) is rewritten as

$$\dot{\hat{z}} = (\hat{A} - \hat{K}\hat{C})\hat{z} + \hat{K}y \tag{28a}$$

$$\hat{y} = \hat{C}\hat{z} \tag{28b}$$

The system matrices $\hat{A}$, $\hat{C}$ and the filter gain $\hat{K}$ of an analytical model need to be distinguished from those of the actual structure, i.e., A, C and K. Using the scheme in Section 3.1, the transfer function from the actual load $T_e(s)$, and the transfer function from the noise $T_\eta(s)$, to estimated loads can be expressed as follows:

$$T_e(s) = B^+\hat{K}(I - \hat{C}(sI - \hat{A} + \hat{K}\hat{C})\hat{K})(C(sI - A)B + D \tag{29a}$$

$$T_\eta(s) = B^+\hat{K}(I - \hat{C}(sI - \hat{A} + \hat{K}\hat{C})\hat{K}) \tag{29b}$$

Fig. 5 shows the transfer function $T_e(s)$ formulated in Eq. (29a) for an error estimate of +5, 0, and −5 percent in the natural frequency for the acceleration response. It is observed that the transfer functions with an error of ± 5 percent have peaks near the natural frequency and are even amplified in the frequency range below the natural frequency. This implies that the actual load is transferred to estimated load as distorted by the error in the low frequency region. On the other hand, the transfer functions from the actual load to the estimated load demonstrates the effect of discrepancies in damping ratios

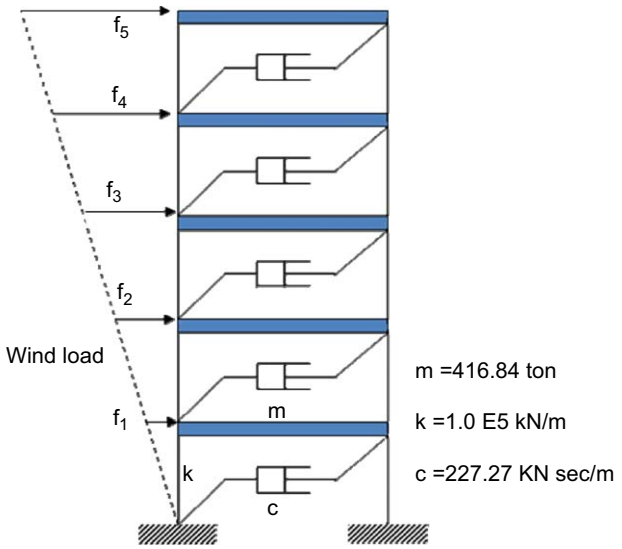

Fig. 7. Model wind excited structure for numerical verification.

(1(exact), 0.5, 2 percent) as shown in Fig. 6. It is noted that the transfer functions $T_e(s)$ are unity in most of the frequency range except around the natural frequency.

4. Numerical verification of the modal wind load

The estimation method is verified using the numerical analysis of a SDOF system subjected to a sinusoidal load and for a MDOF system to dynamic wind loads, respectively. The sinusoidal input having the forcing frequency equal to that of the SDOF system (Load 1) is used as the external load for the SDOF system with dynamic properties given in Table 3. In the case of a MDOF system, the dynamic wind loads (Load 2) applied on each DOF of model structure are shown in Fig. 7. Their fluctuations have been generated from a band pass filter whose salient features are given in Table 4. For the sake of simplicity, it is assumed that the loads are statistically independent of each other and the magnitude of the loads linearly increases with height. The cutoff frequency of the band pass filter is designed on the basis that wind load acting on the structure excites the low frequency ranges in the vicinity of the first and the second natural frequency. Fig. 8 illustrates the spectrum of the wind load applied on the third DOF and its comparison with the original band pass filter prior to scaling, i.e., the maximum amplitude of the load is normalized as unit. It can be seen that the energy density of the load is high near the first modal frequency range but it is wide enough to excite the higher modes.

The noise is obtained from the high pass filter and scaled with respect to the magnitude of responses. The transfer function for the high pass filter and band pass filter is represented in Tables 3 and 4, respectively.

The verification process for the estimated external load is summarized below:

Step 1: Sinusoidal load is generated with the same frequency as that of the SDOF system and wind load and noise are generated from low and high pass filters, respectively. The wind load acting on each DOF is transformed to modal wind load using the modal matrix. The generated load in this step is called ‘the exact load’.

Step 2: Analyze the model structures (SDOF and MDOF) in Tables 3 and 4 subjected to the external load generated in step 1 and estimate acceleration response. The number of accelerometers is determined by the POD method and the modal acceleration responses are calculated using the Eq. (6).

Step 3: Add the noise generated in step 1 into the response chosen in step 2 and estimate the external load using the methodology proposed. The noise level and the uncertainty of dynamic properties are considered in this Step. The external load estimated in this Step is called ‘the estimated load’.

Step 4: Verify the estimation method by comparing ‘the exact load’ and ‘the estimated load’ in time and frequency domains.

4.1. Estimation of the sinusoidal load (Load 1)

First example concerns the estimation of the sinusoidal input Load 1 using the acceleration feedback. Fig. 9 compares the time histories of the estimated forces for Load 1 with different magnitudes of noise when $\gamma = 10^{-8}$. The maximum value of the noise is scaled to be 1 and 3 percent of the maximum response. It can be observed that noise influences on the estimated load depending on its magnitude. It was also observed in Fig. 4 that the noise is transmitted into the estimated

Table 4
Dynamic properties of a MDOF system and Load 2.

Structure	Specification				
Story mass	416.84 t				
Story damping	227.27 kN s/m				
Story stiffness	1.0 E5 kN/m				
Modal properties					
Mode	First	Second	Third	Fourth	Fifth
Mass (t)	1.170	1.385	2.007	3.922	14.442
Damping (percent)	0.5	1.46	2.31	2.96	3.38
Frequency (Hz)	0.70	2.048	3.228	4.147	4.731
Mode shape					
1 floor	**0.2846**	**−0.8308**	**1.3097**	−1.6825	1.9190
2 floor	0.5462	−0.1088	0.3728	1.3979	−3.2287
3 floor	**0.7635**	**−0.5944**	**−1.2036**	0.5211	3.5133
4 floor	0.9190	0.3097	−0.7154	−1.8308	−2.6825
5 floor	**1.0000**	**1.0000**	**1.0000**	1.0000	1.0000
Analysis condition	Time interval: 0.01 s, Total time: 600 s				
Load 2					
Shape	Band pass filter				
Cut off frequency of the band pass filter	0.1–2.0 Hz				
Transfer function of the band pass filter	$\frac{(1.091\times10^{-5}\ s^8+0.003176\ s^7+0.8245\ s^6+96.75\ s^5)+2.041\times10^4\ s^4-0.001038\ s^3-0.0004941\ s^2-0.0005185\ s+0.02413)}{(s^8+31.22\ s^7+518.9\ s^6+5{,}197\ s^5+2.849\times10^4\ s^4+4.113\times10^4\ s^3+3.246\times10^4\ s^2+1.544\times10^4\ s+3351)}$				

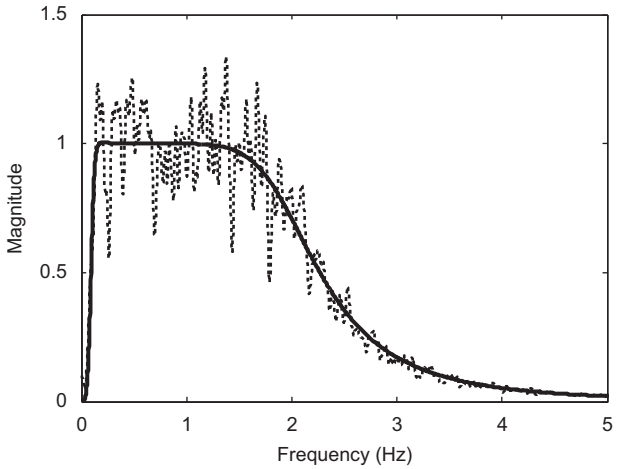

Fig. 8. The spectra of the band pass filter and the generated load (solid line: band pass filter, dotted line: generated load).

load without amplification in the high frequency range for the acceleration feedback. The estimated loads resulting from the displacement and velocity feedbacks are omitted because the noise impairs estimation of loads. Fig. 10 compares the spectra of the estimated forces with two different noise levels to the spectrum of the exact Load 1.

Figs. 11 and 12 show the time histories of the estimated forces for Load 1 with the discrepancy in natural frequency and damping ratio, respectively. The error in the natural frequency was set to be ±5 percent and the damping ratio is assumed to be 1 (exact), 0.5 and 2 percent. It can be observed that the amplitude and phase of the estimated load is affected (Fig. 11) when the natural frequency is modeled incorrectly. Meanwhile the estimated load is simply amplified proportional to the ratio of the assumed damping to the actual damping without phase lag in Fig. 12.

4.2. Estimation of the wind load (Load 2)

In this second example, the modal wind load (Load 2) is estimated using the acceleration feedback. In order to determine the number of sensors, the singular value decomposition (SVD) is performed for the 5×5 dimensional covariance matrix constructed by the analyzed acceleration responses of the model structure. The singular value and corresponding energy contribution by POD method is presented in Table 5. Table 5 gives that the energy contribution of the

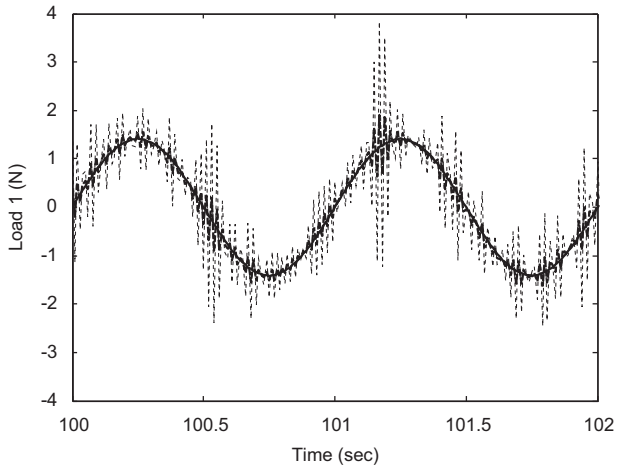

Fig. 9. Time histories of estimated loads for Load 1 case with different noise levels (solid line: exact, dashed line: 1% noise, dotted line: 3% noise).

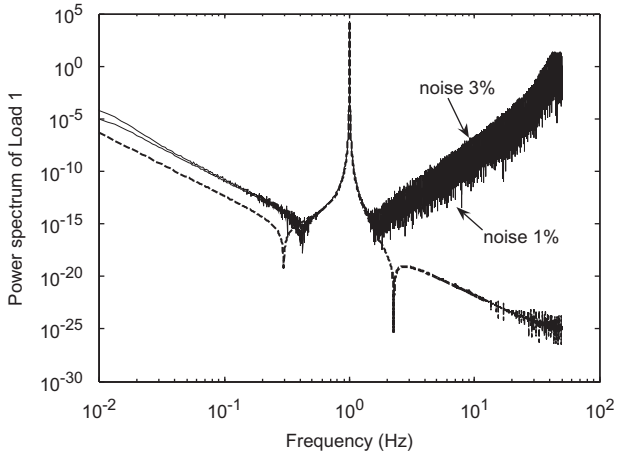

Fig. 10. The spectra of estimated loads for Load 1 case with different noise levels (dashed line: exact, dotted line: 1% noise, solid line: 3% noise).

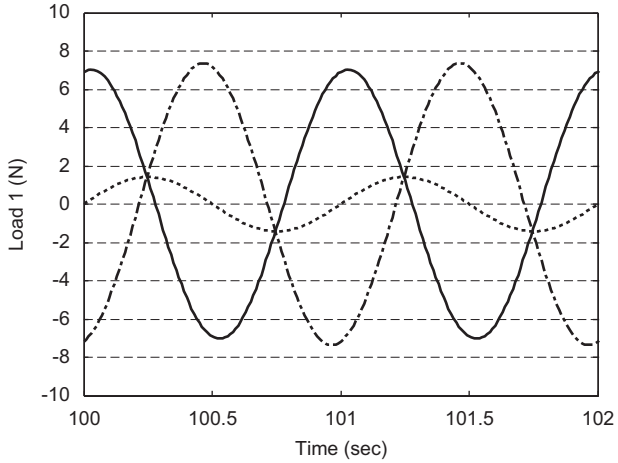

Fig. 11. Time histories of estimated loads for Load 1 case with discrepancy in estimated natural frequency (dotted line: exact, dashed line: +5% discrepancy, solid line: −5% discrepancy).

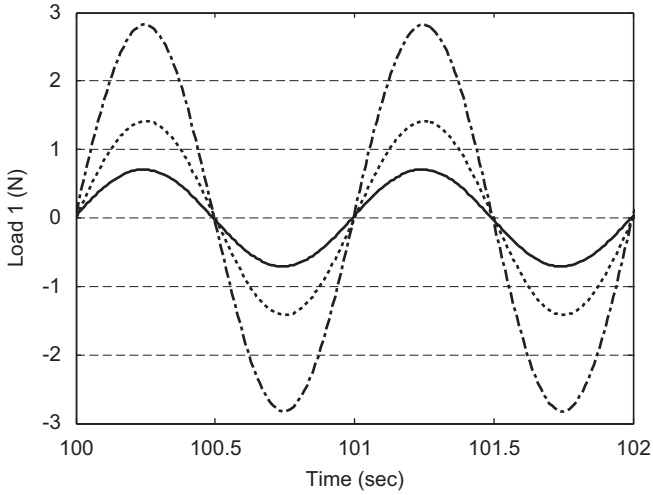

Fig. 12. Time histories of estimated loads for Load 1 case with discrepancy in damping ratio (dotted line: 1% damping (exact), solid line: 0.5% damping, dashed line: 2% damping).

Table 5
The singular value and the energy contribution.

The order of singular value	Singular value of the covariance matrix (10^{-3})	Cumulative sum of singular values (10^{-3})	Energy contribution (percent)
First mode	12.9063	12.9063	86.60
Second mode	1.9148	14.8211	99.45
Thirdrd mode	0.0668	14.8879	99.90
Fourth mode	0.0114	14.8993	99.98
Fifth mode	0.0033	14.9026	100

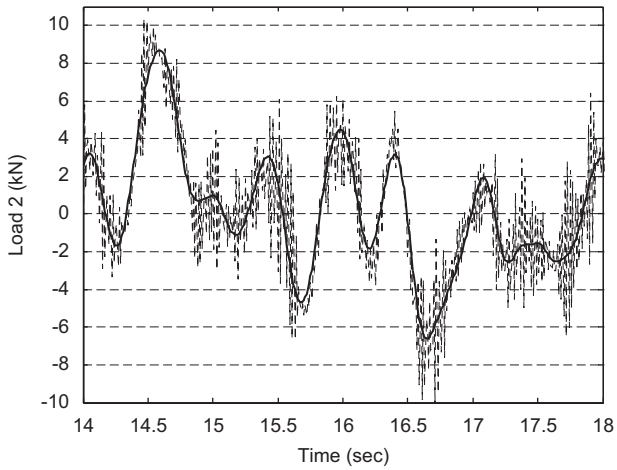

Fig. 13. Time histories of estimated loads for Load 2 case with different noise levels (solid line: exact, dotted line: 10% noise).

first mode is 12.9063×10^{-3}, the second mode is 1.9148×10^{-3} and the summation of the two mode's energy contribution is over 99 percent. Considering the energy contribution of the two modes, the number of accelerometers is determined to be three.

The first modal wind load is identified from the first modal acceleration response which is calculated by Eq. (15) with the 3×3 dimensional eigenmatrix given in bold in Table 4 and the accelerations obtained from accelerometers installed at the first, third and fifth floor. The optimal sensor location is not investigated here. Figs. 13 and 14 compare the exact load to the estimated loads in the time and frequency domains for three different noise levels of which maximum value are scaled

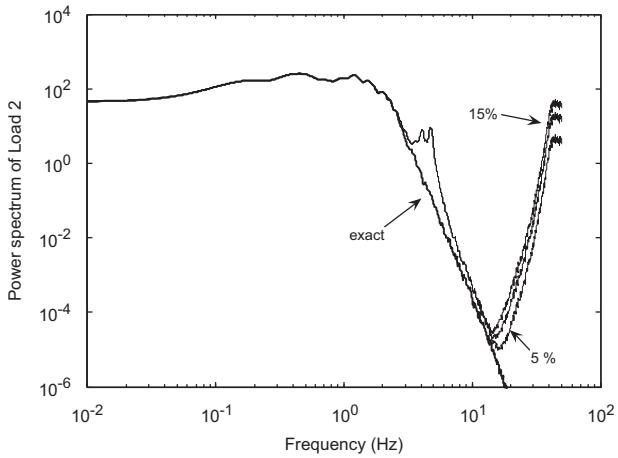

Fig. 14. The spectra of estimated loads for Load 2 case with different noise levels. (The two peaks between 4–5 Hz are induced by the fourth and fifth modal acceleration responses which were not separated from the measured acceleration response.)

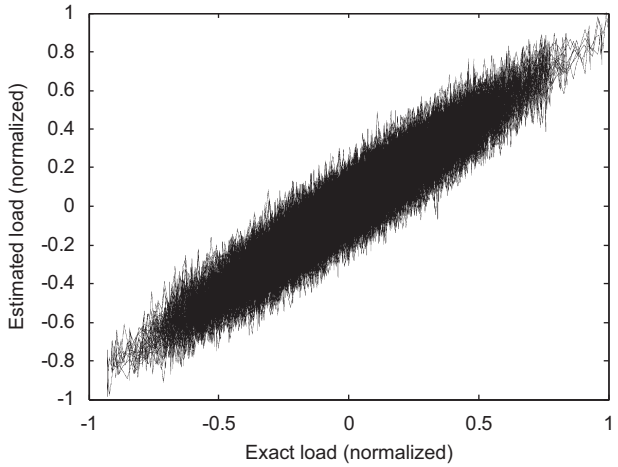

Fig. 15. Correlogram between the actual and estimated loads. (Noise level = 5%, Correlation coefficient = 0.931.)

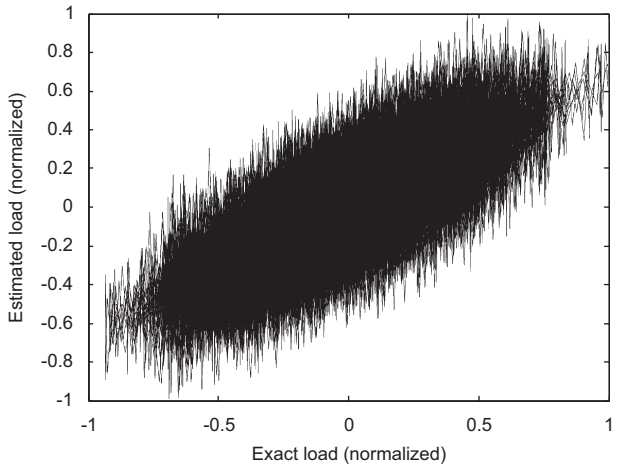

Fig. 16. Correlogram between the actual and estimated loads. (Noise level = 15%, Correlation coefficient = 0.687.)

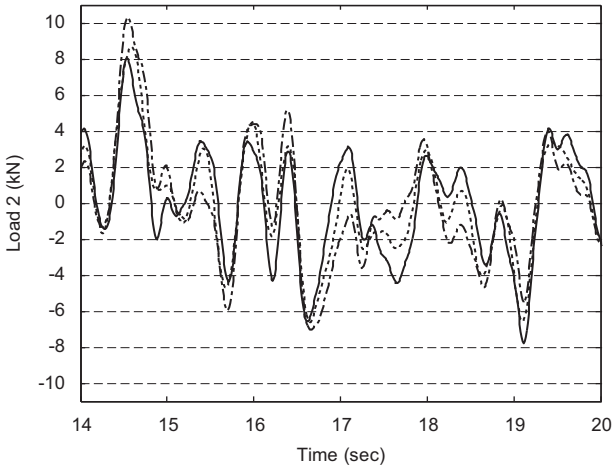

Fig. 17. Time histories of estimated loads for Load 2 case with discrepancy in natural frequency (dotted line: exact, solid line: −5% discrepancy, dashed line: +5% discrepancy).

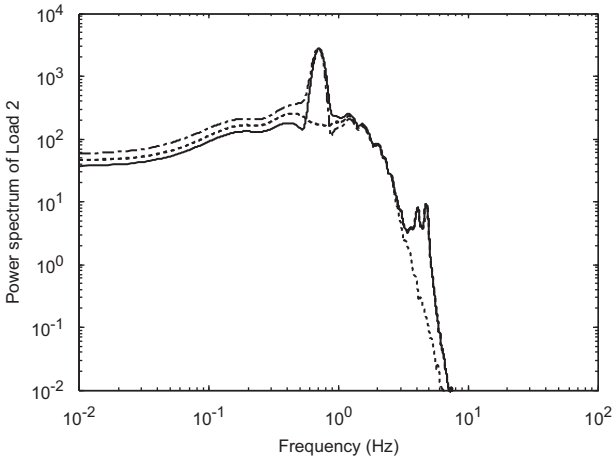

Fig. 18. The spectra of estimated loads for Load 2 case with discrepancy in natural frequency (dotted line: exact, solid line: −5% discrepancy, dashed line: +5% discrepancy).

to be 5, 10 and 15 percent of the maximum acceleration response, respectively. Similar to the result in the first example, the level of noise influences the estimated load. However, it can be observed in Figs. 9 and 13 that the effect of the noise included in the acceleration response is not significant in the case of dynamic wind load (Load 2) when compared to the sinusoidal load case (Load 1). This can be explained by the fact that the magnitude of the acceleration response induced by Load 2 is much lower than that induced by the Load 1 in which resonance takes place. In other words, the magnitude of noise included in the Load 1 is much larger than that included in the Load 2 if the ratio of the noise to the response is the same. It can be observed in Fig. 14 that the effect of noise becomes significant in high frequency range. In Fig. 14, the two peaks between 4 and 5 Hz appear that are induced by the fourth and fifth modal acceleration response, which are not separated from measured acceleration response. Figs. 15 and 16 show the correlograms between the exact and the estimated loads for two different noise levels. The results demonstrate that the correlation coefficient decreases as the noise level increases.

Figs. 17 and 18 compare the estimated load with the exact Load 2 in the time and frequency domains, respectively, for ± 5 percent errors in natural frequency. It can be observed in Fig. 17 that the 5 percent error in the natural frequency induces a slight difference in the estimated loads. It can also be observed in Fig. 18 that the spectra of the estimated load are slightly different from that of the exact load below natural frequency and a peak occurs near the natural frequency. The correlograms between the exact load and the estimated load are shown in Figs. 19 and 20 in case that the error of natural frequency is 0 and 5 percent, respectively. Fig. 19 demonstrates that the external load can be estimated with greater reliability when there is no error in the frequency estimates. However, 5 percent error renders a lower level of correlation between the estimated and the exact loads (Fig. 20). The noise and the discrepancy of natural frequency both apparently

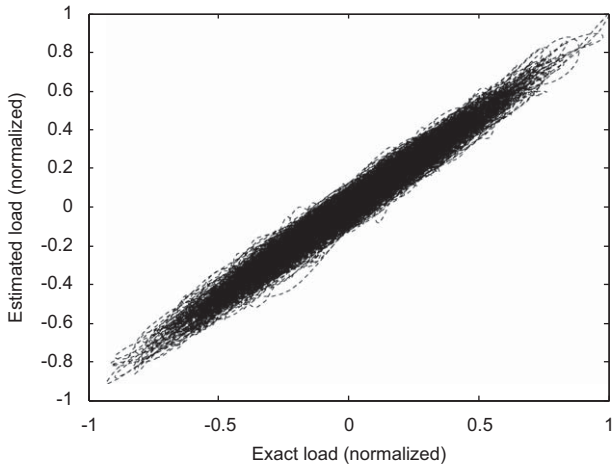

Fig. 19. Correlogram between the actual and estimated loads. (The error of natural frequency = 0%, Correlation coefficient = 0.985.)

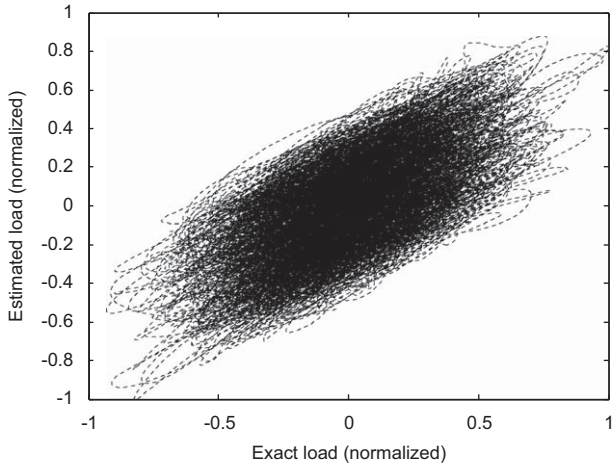

Fig. 20. Correlogram between the actual and estimated loads. (The error of natural frequency = 5%, Correlation coefficient = 0.682.)

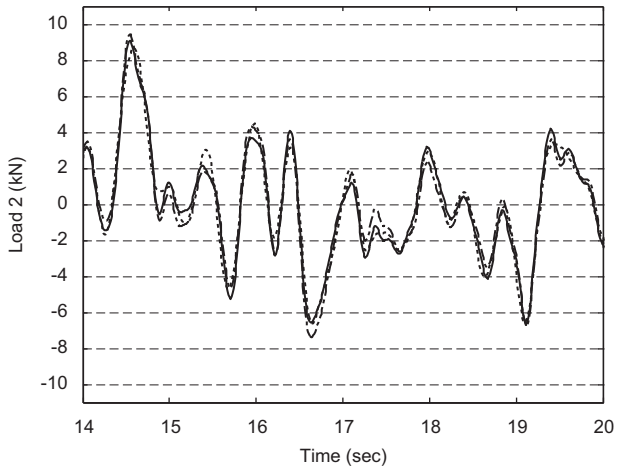

Fig. 21. Time histories of estimated loads for Load 2 case with discrepancy in damping ratio (dotted line: 0.5% damping (exact), solid line: 0.05% damping, dashed line: 2.5% damping).

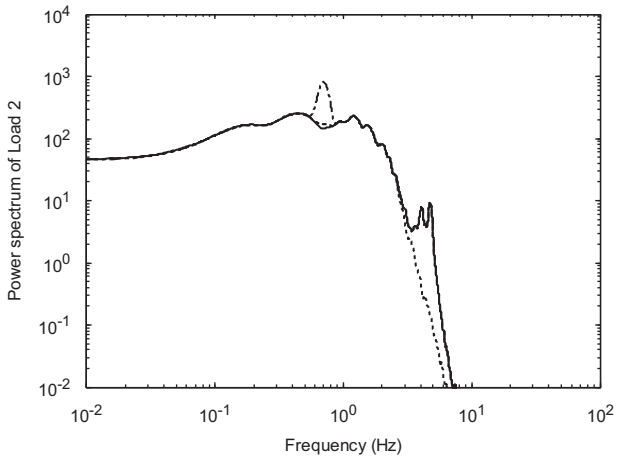

Fig. 22. The spectra of estimated loads for Load 2 case with discrepancy in damping ratio (dotted line: 0.5% damping, solid line: 0.05% damping, dashed line: 2.5% damping).

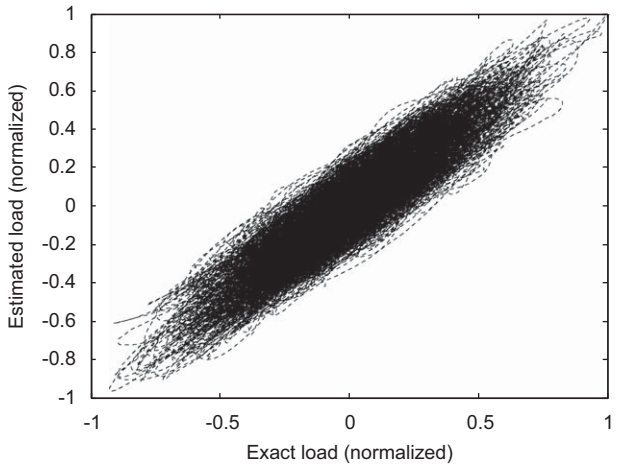

Fig. 23. Correlogram between the actual and estimated loads. (The damping ratio = 2.5%, Correlation coefficient = 0.918.)

have a notable influence on the estimation of external loads, but the trends are a bit different when comparing the correlograms in Figs. 16 and 20. It is observed from Fig. 16 that the estimated load may be expressed as the sum of the exact load and the noise. Meanwhile, the same trend is not observed in Fig. 20 where there is an apparent bias in the estimated load.

For damping ratio discrepancies of 0.05 and 2.5 percent, the estimated loads are compared with the exact Load 2 in the time and frequency domains in Figs. 21 and 22, respectively. These figures suggest that the discrepancy in the damping ratio does not affect the estimated load except a peak that occurred near the natural frequency in the spectra. It can be also noted in Fig. 23 that the estimated load is very close to the exact load with a correlation coefficient of 0.918.

From the analysis results it is found that the errors in dynamic properties do not affect the estimated force significantly for Load 2. This is quite different from the case of the Load 1, which is very sensitive to the error in dynamic characteristics because the input is composed of only one frequency component at the system natural frequency. Compared to the case of Load 1, the estimates of force for Load 2 are relatively insensitive to the error because these are composed of a relatively broad band of frequencies.

5. Conclusions

In this study an analytical procedure is derived based on the Kalman filtering scheme to estimate external loads applied on a structure using the attendant structural response. The estimation methodology is formulated in a closed-form for a SDOF system in modal space. The influence of various variables such as the type of response, the magnitude of noise and

discrepancy in the estimation of dynamic properties on the estimated load is evaluated in both time and frequency domains.

Transfer functions that relate the actual load to the estimated load show that the velocity feedback rather than the displacement or acceleration feedback is the most stable in the estimation of external load. However, considering that the noise is amplified in displacement and velocity feedbacks, the acceleration feedback is preferable for the estimation of external loads. In the acceleration feedback, the noise included in the acceleration response is reflected in the estimated load without any amplification in the frequency range higher than structural natural frequency.

It is observed that the discrepancy in the estimation of dynamic characteristics between an analytical model and the prototype structure causes the transfer function from the exact load to the estimated load to be distorted near and below the natural frequency. The discrepancy in estimation of natural frequency results in a difference in the phase angle of the transfer functions, whereas a discrepancy in the damping ratio does not affect the transfer function to the same level as the discrepancy in the natural frequency except near the natural frequency. The estimation of external force for structures excited by a random load is relatively insensitive to the error in the estimation of structural dynamic features and external noise whereas the estimated force is very sensitive to these errors for sinusoidal input.

Acknowledgments

This research was supported by a Grant (05RCB05-01) from Regional Technology Innovation Program (RTIP) funded by Ministry of Land, Transportation and Maritime Affairs (MLTM) of Korean government and this work was also supported by the Korean Ministry of Education, Science and Technology Grant (The Regional Core Research Program/Biohousing Research Institute). The work was in part also supported by NSF Grant #CMMI 06–01143.

References

[1] Y. Zhou, T. Kijewski-Correa, A. Kareem, Along-wind load effects on tall buildings: comparative study of major international codes and standards, *ASCE Journal of Structural Engineering* 128 (6) (2002) 788–796.
[2] Structural Engineering Institute of the American Society of Civil engineers, Minimum design loads for buildings and other structures, SEI/ASCE 7-05 (ASCE standard), ASCE, 2005.
[3] NRCC, User's Guide-NBC1995 Structural Commentaries (Part 4), 1996.
[4] Architectural Institute of Japan, Recommendations for loads on buildings, 1996.
[5] I. Goswanmi, R.H. Scanlan, N.P. Jones, Vortex induced vibration of circular cylinders. I: experimental data, *Journal of Engineering Mechanics* 119 (11) (1993) 2270–2287.
[6] A. Kareem, Fluctuating wind loads on buildings, *ASCE Journal of the Engineering Mechanics Division* 108 (6) (1982) 1086–1102.
[7] D. Williams, R.P.N. Jones, Dynamic loads in aeroplanes under given impulsive loads with particular reference to landing and gust loads on a large flying boat, Aeronautic Research Council, Technical Report No. 2221, 1948.
[8] K.K. Stevens, Force identification problems-an overviews, *Proceedings of the* 1987 *SEM Spring Conference on Experimental Mechanics*, Houston, TX, USA, 1987, pp. 14–19.
[9] S.S. Law, J.Q. Bu, X.Q. Zhu, Time-varying wind load identification from structural responses, *Engineering Structure* 27 (2005) 1586–1598.
[10] Z.R. Lu, S.S. Law, Force identification based on sensitivity in time domain, *Journal of Engineering Mechanics* 132 (10) (2006) 1050–1056.
[11] Y. Liu, W.S. Shepard Jr., Dynamic force identification based on enhanced least squares and total least-squares schemes in the frequency domain, *Journal of Sound and Vibration* 282 (2005) 37–60.
[12] T.H.T. Chan, S.S. Law, T.H. Yung, An interpretive method for moving force identification, *Journal of Sound and Vibration* 219 (3) (1999) 503–524.
[13] X.Q. Zhu, S.S. Law, Practical aspects in moving load identification, *Journal of Sound and Vibration* 258 (1) (2002) 123–146.
[14] L. Yu, T.H.T. Chan, Recent research on identification of moving loads on bridges, *Journal of Sound and Vibration* 305 (2007) 3–21.
[15] J.J. Liu, C.K. Ma, I.C. Kung, D.C. Lin, Input force estimation of a cantilever plate by using a system identification technique, *Computer Methods in Applied Mechanics and Engineering* 190 (2000) 1309–1322.
[16] C.K. Ma, J.M. Chang, D.C. Lin, Input forces estimation of beam structures by an inverse method, *Journal of Sound and Vibration* 259 (2) (2003) 387–407.
[17] C.K. Ma, C.C. Ho, An inverse method for the estimation of input forces acting on non-linear structural system, *Journal of Sound and Vibration* 275 (2004) 953–971.
[18] M.S. Grewal, A.P. Andrews, *Kalman Filtering Theory and Practice*, Prentice-Hall, Englewood Cliffs, NJ, 1993.
[19] T.T. Soong, *Active Structural Control: Theory and Practice*, Addison-Wesley, Reading, MA, 1991.
[20] Y.C. Liang, H.P. Lee, S.P. Lim, W.Z. Lin, K.H. Lee, C.G. Wu, Proper orthogonal decomposition and its applications—part I: theory, *Journal of Sound and Vibration* 252 (2002) 527–544.
[21] X. Chen, A. Kareem, Proper orthogonal decomposition-based modeling, analysis, and simulation of dynamic wind load effects on structures, *ASCE Journal of Engineering Mechanics* 131 (4) (2005) 325–339.
[22] J.S. Hwang, H. Kim, J. Kim, Estimation of the modal mass of a structure with a tuned-mass damper using H-infinity optimal model reduction, *Engineering Structures* 28 (2006) 34–42.
[23] J.M.W. Brownjohn, A. Pavic, Experimental methods for estimating modal mass in footbridges using human-induced dynamic excitation, *Engineering Structures* 29 (2007) 2833–2843.
[24] T. Kijewski-Correa, J. Kilpatrick, A. Kareem, D.K. Kwon, R. Bashor, M. Kochly, B.S. Young, A. Abdelrazaq, J. Galsworthy, N. Isyumov, D. Morrish, R.C. Sinn, W.F. Baker, Validating the wind-induced response of tall buildings: a synopsis of the Chicago full-scale monitoring program, *ASCE Journal of Structural Engineering* 132 (10) (2006) 1509–1523.